Layer-by-layer assembly of gold nanoparticles with titania nanosheets: control of plasmon resonance and photovoltaic properties

Nobuyuki Sakai,[a] Takayoshi Sasaki,[b] Kazuki Matsubara[a] and Tetsu Tatsuma*[ac]

Received 24th January 2010, Accepted 10th March 2010
First published as an Advance Article on the web 12th April 2010
DOI: 10.1039/c0jm00135j

Layer-by-layer assembled multilayer films composed of gold nanoparticles (Au NPs) and titania nanosheets were constructed on a glass or ITO substrate in an arbitrary layering order. Coverage of Au NPs with 1 to 3 layers of titania nanosheets enhances their plasmon resonance-based absorption and photocurrents. Absorption can be improved further by alternate stacking of Au NPs and titania nanosheets. Plasmon resonance of the multilayer can be enhanced and redshifted by interlayer plasmon coupling *via* a single intervening nanosheet layer, whereas the coupling can be suppressed, if necessary, by two or more layers of nanosheets. Direction of the photocurrents can also be switched; annealed ITO/titania nanosheet/Au NP electrodes exhibit anodic photocurrents and annealed ITO/Au NP/titania nanosheet electrodes exhibit cathodic photocurrents.

Introduction

Gold and silver nanoparticles (Au and Ag NPs) exhibit localized surface plasmon resonance (LSPR).[1] The resonance wavelength depends on the size, shape, interparticle distance and refractive index of the surrounding medium. Such metal NPs have been widely applied to LSPR sensors,[2] surface-enhanced Raman scattering (SERS),[3] surface-enhanced infrared absorption spectroscopy (SEIRAS),[4] imaging,[5] multicolour photochromism,[6] photoelectric conversion,[7] visible-light responsive photocatalysis[7b,e,8] and photoinduced volume changes of gels.[9] For these applications, it is frequently required to immobilize and/or integrate the NPs on substrates, and various methods have been developed such as anchoring *via* thiols and silane coupling agents,[10] electrochemical deposition,[11] photocatalytic deposition[6,7b,9] and layer-by-layer assembly.[12]

Among them, the layer-by-layer assembly utilizing electrostatic interaction[13] can control the adsorbed amount[12c,f] as well as the interparticle distance[12e] by changing the deposition time and/or repeating the deposition cycle. The interparticle spacing is an important factor dictating interparticle plasmon coupling. The plasmon coupling, which is characterized by redshifted resonance wavelength and enhanced absorption, scattering, and local electric field, is often observed when the spacing is comparable to or smaller than the particle diameter.[14] The coupling is useful for, for instance, sensitized sensing, second harmonic generation (SHG), and SERS, whereas redshifted and broadened LSPR bands due to the coupling are undesirable in some applications. Also, the layer-by-layer technique allows the coating of metal NPs with an ultrathin layer of a finely regulated thickness to protect the NPs or enhance their LSPR. Thus, this sophisticated method is beneficial for tuning the plasmon coupling and enhancing LSPR, and has been applied to LSPR sensors,[12b,e] SHG,[15] SERS[3b,c] and dye-sensitized solar cells.[12g]

As a counterpart of metal NPs in the layer-by-layer assembly, organic compounds are employed in general. However, oxide nanosheets[16] such as titanium oxide,[17] which are obtained by delaminating the layered oxides into each layer, are also promising candidates for their stability and excellent semiconducting properties. The oxide nanosheets have been assembled by layer-by-layer assembly with polyions such as polymers, metal complexes, oxide clusters and oppositely charged nanosheets.[16] Since the oxide nanosheets are as thin as 1 nm regardless of the lateral dimensions of several hundred nanometres to tens of micrometres, the interparticle distance and the coating thickness can be controlled on the 1 nm scale. Although the assemblies of Au and Ag NPs with titania nanosheets have been reported,[18] there are no reports regarding the modulation of plasmon resonance by integrating metal NPs with oxide nanosheets.

In the present work, we have fabricated layered nanostructures consisting of Au NPs and titania nanosheets, which have a high refractive index, in an arbitrary layering order and have examined the effects of titania nanosheets on the LSPR properties and a LSPR-based functionality of Au NPs. We have found that the LSPR is significantly enhanced by covering Au NPs with one or two layers of titania nanosheets. Interparticle plasmon coupling is at its maximum *via* a single intervening nanosheet layer, whereas three or more layers suppress the coupling almost completely. These results suggest that the decay length of electric field away from the Au NP surface is the thickness of the two to three nanosheet layers. We have also reported that Au NPs adsorbed on TiO_2 and those covered with TiO_2 generate anodic and cathodic photocurrents, respectively, on the basis of LSPR.[7] In the present layered nanostructures, the photocurrent increases as the LSPR is enhanced by covering with titania nanosheets. In addition, the polarity of photoresponses is controlled by changing the layering order of Au NPs and titania nanosheets.

[a]*Institute of Industrial Science, The University of Tokyo, 4-6-1 Komaba, Meguro-ku, Tokyo, 153-8505, Japan. E-mail: tatsuma@iis.u-tokyo.ac.jp; Tel: +81 3-5452-6336; +81 3-5452-6338*
[b]*International Center for Materials Nanoarchitectonics, National Institute for Materials Science, 1-1 Namiki, Tsukuba, Ibaraki, 305-0044, Japan*
[c]*PRESTO, Japan Science and Technology Agency (JST), 4-1-8 Honcho, Kawaguchi, Saitama, 332-0012, Japan*

Experimental

Synthesis of colloidal solutions

A colloidal solution of 3.5 nm citrate-stabilized Au NPs was prepared according to literature.[19] An ice-cold solution (0.6 cm^3) of 0.1 mol dm^{-3} $NaBH_4$ (95%) was added into 20 cm^3 of aqueous solution containing 2.5×10^{-4} mol dm^{-3} $HAuCl_4$ (99%) and 2.5×10^{-4} mol dm^{-3} trisodium citrate (99%) under vigorous stirring. The colorless solution became red, suggesting the formation of Au NPs, and was kept for 1–2 days before use. Titania ($Ti_{0.91}O_2$) nanosheets were synthesized by a well-established procedure reported previously.[17] Briefly, a stoichiometric mixture of Cs_2CO_3 (95%) and TiO_2 (99.9%) was calcined at 800 °C for 20 h to synthesize layered caesium titanates, $Cs_{0.7}Ti_{1.825}\square_{0.175}O_4$ (□: vacancy at Ti octahedral site).[20] Subsequent acid leaching converted them into protonated forms of $H_{0.7}Ti_{1.825}\square_{0.175}O_4 \cdot H_2O$. The resulting protonic product (0.4 g) was shaken vigorously in 100 cm^3 of a 1.7×10^{-2} mol dm^{-3} tetra-*n*-butylammonium hydroxide solution at ambient temperature. The resulting suspension with an opalescent appearance contained well-dispersed exfoliated titania nanosheets (~1 nm in thickness and 0.1–1 μm in lateral size).[17c] The titania nanosheets are negatively charged due to vacancies at octahedral Ti sites.

Fabrication of multilayer assembled films

Pyrex glass substrates were cleaned by ultrasonic treatment in detergent and pure water for 30 min each followed by washing with ultrapure water. The substrate was first immersed in a polyethylenimine (PEI, $M_w = \sim 7.5 \times 10^5$) solution (1.25 g cm^{-3}, pH 9) to introduce positive charges onto the surface. The titania nanosheets and poly(diallyldimethylammonium) chloride (PDDA, $M_w = \sim 1 \times 10^5$ to 2×10^5) were sequentially adsorbed from the colloidal suspension of titania nanosheets (0.08 g dm^{-3}, pH 9) and a PDDA solution (20 g dm^{-3}, pH 9), respectively. The Au NPs were deposited by immersing the substrate, glass/PEI/$Ti_{0.91}O_2$/PDDA, into their colloidal solution (0.048 g dm^{-3}, pH 9). A poly(sodium 4-styrenesulfonate) (PSS, $M_w = \sim 7 \times 10^4$) solution (7 g cm^{-3}, pH 1.5) instead of titania nanosheets was also used to introduce negative charges onto the surface. The substrate was immersed in each solution for 20 min, or otherwise noted, and then rinsed thoroughly with ultrapure water.

Film characterizations

A spectrophotometer (V-560, JASCO) was employed to record UV-vis absorption spectra for films fabricated on glass substrates. An atomic force microscope (NanoNavi Station, Seiko Instruments) was used to examine the surface morphology of the multilayer films. The measurements were carried out in a tapping mode with a driving frequency of 110–140 kHz at a scan rate of 0.4 Hz by using a silicon cantilever with a normal spring constant of ~15 N m^{-1} (SI-DF20, Seiko Instruments). Lateral diameters measured were corrected by taking a tip curvature radius (~10 nm) and cone angle (~34°) into account on the assumption that the particles are spherical. X-ray diffraction (XRD) data were collected using a powder diffractometer (Rint 2100, Rigaku) with monochromatized Cu-Kα radiation ($\lambda = 0.15405$ nm), operated at 40 kV and 40 mA.

Photoelectrochemical investigation

Photoelectrochemical measurements were carried out in a conventional three-electrode, single-compartment glass cell, using a Solartron SI 1287 potentiostat. Multilayer films assembled on conductive ITO-coated glass substrates served as the working electrode. The counter and reference electrodes were a platinum wire and $Ag|Ag^+$, respectively. A N_2-saturated acetonitrile solution containing 0.01 mol dm^{-3} tetra-*n*-butylammonium perchlorate (TBAP) and 0.74 mol dm^{-3} triethanolamine (TEOA) was employed as an electrolyte. Photocurrent was measured at rest potential under visible light (monochromatic or $460 < \lambda < 700$ nm), which was irradiated from the back of the working electrode using a 150 W Xe lamp (LA-410UV-3, Hayashi Watch-Works) through a band pass filter (F10 series, CVI Laser; fwhm = 10 nm) or a sharp cut filter (SCF-50S-48Y, Sigma Koki), respectively. The light intensity was adjusted to ~4 or 200 mW cm^{-2} by using a radiant power meter (Model 70260, Oriel) equipped with a silicon probe (Model 70282, Oriel) or a low noise thermopile probe (Model 70261, Oriel), respectively.

Results and discussion

Adsorption of Au NPs onto titania nanosheets

We examined the adsorption characteristics of the citrate-stabilized Au NPs onto substrates covered with titania nanosheets in a layer-by-layer fashion by monitoring UV-vis absorption spectra. When a PEI-coated glass plate was immersed in the colloidal suspension of titania nanosheets for 20 min, the absorption peak at 260 nm, which is based on the band gap excitation of titania nanosheets, appeared as reported previously.[21] Although the Au NPs did not adsorb on the negatively charged, titania nanosheet-coated substrates, the adsorption was observed, as indicated by appearance of a LSPR-based absorption peak at 539 nm, after further coating of the substrates with a positively charged PDDA layer. This is reasonable because the citrate-stabilized Au NPs are negatively charged in their colloidal solutions. When the immersion time was prolonged from 2 min up to 72 h, the LSPR-based absorption peak was enhanced and redshifted from 539 to 660 nm (Fig. 1). Accordingly, the colour of the films changed from pale red to dark blue (Fig. 1b, inset). A second peak at 535 nm appeared after the immersion for 24 h or longer. Similar peaks have been reported for aggregating Au NPs, such as those (30 nm in diameter) immobilized on silane-modified quartz slides[22] and those cross-linked *via* glutathione.[23]

The morphology of Au NPs deposited on the titania nanosheets was examined by the tapping-mode AFM observation. While the two-dimensional sheet-like morphology was observed for the substrates covered with titania nanosheets on the top (Fig. 2a), many spherical particles and the sheet-like morphology behind them, which are assignable to the Au NPs and titania nanosheets, respectively, were found on the substrates after adsorption of Au NPs for 2–20 min (Fig. 2b–d). The sheet-like morphology was completely covered with the spherical particles after adsorption for longer than 160 min (Fig. 2e–h). As the adsorption time was prolonged from 2 min to 72 h, the average diameter and height of the particles increased (corrected lateral diameter $d = 4.4 \pm 4.1$ to 17.0 ± 8.2 nm, height $h = 4.7 \pm 2.0$ to

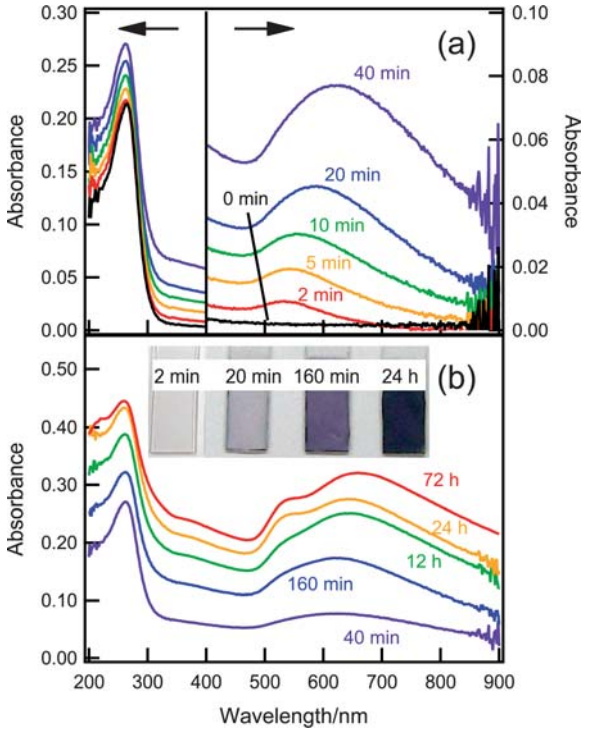

Fig. 1 UV-vis absorption spectra for the glass/PEI/$Ti_{0.91}O_2$/PDDA substrates after immersion into colloidal suspension of Au NPs for a period indicated in the spectra. Inset in panel (b) shows the photographs of selected samples.

14.2 ± 4.8 nm; average ± standard deviation; n = 50–100), as evaluated by cross section analyses. As mentioned below, since XRD peaks became sharper with the immersion time, the Au NPs do not simply aggregate but coalesce into larger ones. It was recently reported that such a size increase of thiol-protected Au NPs is induced even at room temperature in the presence of Brønsted acids and halogen anions such as Br^- and Cl^-.[24] The mechanism has been proposed as follows. The thiolates adsorbed on the gold surface are protonated by the acid and substituted with the halogen anions, which promote the coalescence. In the present case, citrate ions stabilizing Au NPs couple with the cationic PDDA on the substrates and are substituted with the Cl^- ions that were coupled with PDDA, resulting in the coalescence of Au NPs. Although it is known that a size increase of Au NPs often redshifts their plasmon resonance wavelength, a size increase from 4.7 to 14.2 nm does not cause a significant redshift.[25] Hence the aforementioned redshift from 539 to 660 nm is ascribed to the plasmon coupling between adjacent Au NPs. The mean interparticle distance, which was estimated from the surface density and lateral diameter of adsorbed NPs on the assumption that the NPs are ordered hexagonally, decreased from 32.1 to 27.3 nm. The small decrease suggests that the possible enhancement of plasmon coupling is likely due to the increased particle size, since the coupling is dictated by the spacing/diameter ratio.[26] In the following experiments, deposition time for Au NPs was 2 or 20 min (d = 5.3 ± 3.8 nm and h = 5.7 ± 1.9 nm for the latter). The coalescence was observed only in the Au NP solution, but not in the other solutions used in the present work.

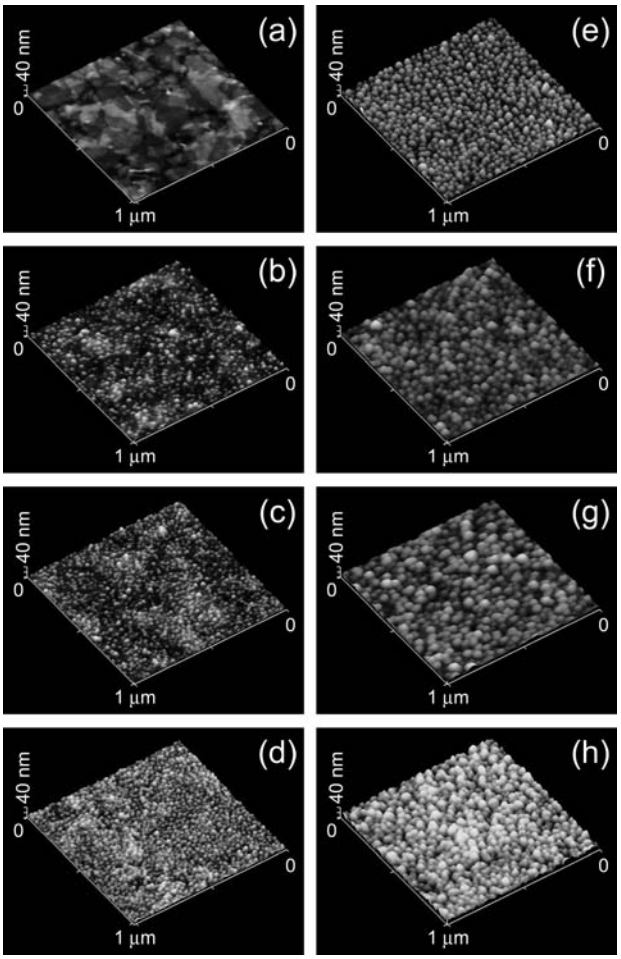

Fig. 2 Tapping-mode AFM images of the films, (a) glass/PEI/$Ti_{0.91}O_2$ and (b–h) glass/PEI/$Ti_{0.91}O_2$/PDDA/Au NP. The deposition time of Au NPs was (b) 2, (c) 5, (d) 20, (e) 160 min, (f) 12, (g) 24, (h) 72 h.

Multilayer assembly of Au NPs and titania nanosheets

The obtained films, glass/PEI/$Ti_{0.91}O_2$/PDDA/Au NP, were covered with another layer of titania nanosheets by employing another PDDA layer as an electrostatic glue. The AFM images are shown in Fig. 3. For some Au NPs, a single corrugated nanosheet covers several neighboring Au NPs, and for the other NPs, each NP is independently covered with a small nanosheet. The corrugation was more significant for the film of 20 min deposition of Au NPs than that for the film of 2 min deposition. The difference may be ascribed to the different interparticle distance (24.9 and

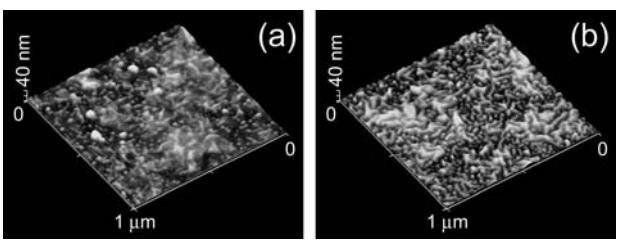

Fig. 3 Tapping-mode AFM images of the films, glass/PEI/$Ti_{0.91}O_2$/PDDA/Au NP/PDDA/$Ti_{0.91}O_2$. The deposition time of Au NPs was (a) 2 and (b) 20 min.

32.1 nm, respectively); it may be easier to wrap a few neighboring NPs within a single corrugation, if the distance is smaller. Anisotropic wrapping of NPs in a titania corrugation is expected to cause anisotropic optical responses as described below.

Similarly, Au NPs were adsorbed on the top titania nanosheet layer by employing another PDDA layer, and the deposition cycle was repeated. The alternate adsorption of Au NPs (deposition time: 2 min) and titania nanosheets enhanced the two absorption peaks at around 540–570 and 260 nm, respectively (Fig. 4a). The increment of absorbance at 260 nm ($\sim$0.127 $\pm$ 0.013 per layer) was comparable to that ($\sim$0.128 per layer) for a multiple stack of titania nanosheet monolayers with intervening PDDA,[21] suggesting that the nanosheets are adsorbed on the Au NPs essentially as a monolayer. The adsorption of the first layer of titania nanosheets on the Au NP layer also enhanced and redshifted the LSPR-based absorption peak from 0.0087 at 539 nm to 0.018 at 552 nm, where the nanosheets intrinsically do not absorb. The observed modulation can be explained in terms of the high refractive index of titania nanosheets ($n = \sim 2$ at 600 nm),[21b] since increasing the refractive index of the surrounding medium enhances and redshifts the LSPR-based absorption of metal NPs.[1] The peak redshifted to $\sim$580 nm after 10 alternate adsorption cycles. Not only the increased local refractive index but also interlayer plasmon coupling must be responsible for this additional redshift.

In the case of 20 min deposition of Au NPs, the increment of absorbance at 260 nm ($\sim$0.136 $\pm$ 0.009 per layer) by the adsorption of titania nanosheets (Fig. 4b) was larger than that of the 2 min deposition films shown above, probably because a larger amount of titania nanosheets adsorbed on the substrate per unit area due to larger overall surface area of Au NPs (Fig. 3b). The adsorption of the first layer of titania nanosheets on the first layer of Au NPs also enhanced and redshifted the broad absorption peak from 0.050 at 592 nm to 0.069 at 598 nm, and the enhancement and redshift were observed after every adsorption of titania nanosheets. It is noted that the absorbance enhancement in this broad plasmon band was more significant in the longer wavelength region, and the average ratio of absorbance increment at 800 nm to that at the peak wavelength was $\sim$1.4, whereas the ratio was $\sim$0.73 in the case of the 2 min deposition films. Such enhancement of plasmon resonance in the longer wavelength region when the Au NPs are covered with titania nanosheets may be ascribed to the anisotropic wrapping of the Au NPs in titania nanosheet corrugations as described above. The anisotropic wrapping causes anisotropic distribution of the local refractive index and changes the optical properties of the spherical Au NPs to those of anisotropic ones.

Apart from the spectroscopic properties, the structural aspects of the multilayer films were examined by XRD. The diffraction patterns for the multilayer films, glass/PEI/$Ti_{0.91}O_2$/PDDA/Au NP/(PDDA/$Ti_{0.91}O_2$/PDDA/Au NP)$_{11}$, showed two distinctive peaks at $2\theta = 5.2$–$5.4°$ and $38.2°$ as well as the halo pattern at 15–30° due to the glass substrates (Fig. 5). The peak at $2\theta = 38.2°$, which is ascribed to the diffraction from the Au(111) face, was enhanced with the increase of the number of layers, confirming the existence of Au NPs inside the films. The mean crystalline size of the Au NPs was estimated from the full width at half-maximum (fwhm) of the diffraction peak by using Scherrer's equation[27] to be 5.3 and 7.0 nm for the samples of 2 and 20 min deposition of Au NPs, respectively, both of which are in good agreement with the particles' height estimated from the AFM images (4.7 $\pm$ 2.0 and 5.7 $\pm$ 1.9 nm, respectively) shown above (Fig. 2). As the deposition time increased further, the diffraction peak became sharper; the particle size was estimated to be 12.5 and 14.2 nm for the deposition time of 24 and 144 h, respectively. These results suggest that the Au NPs do not simply aggregate

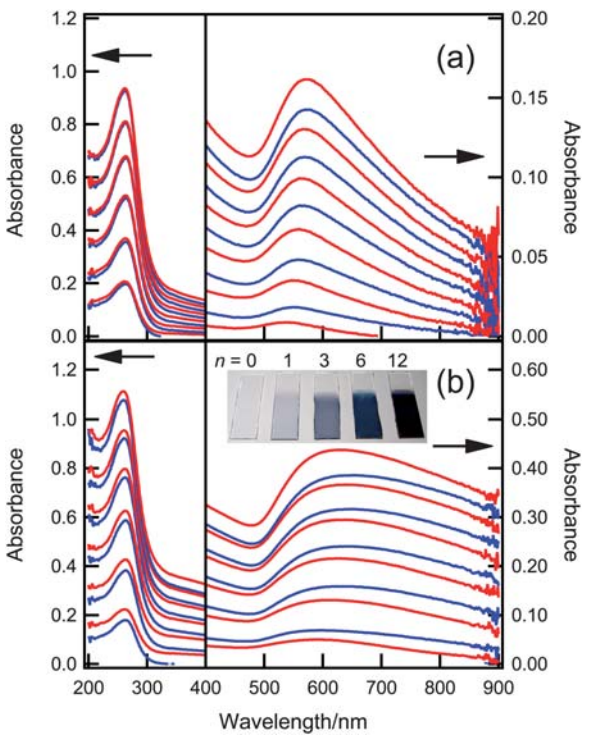

Fig. 4 UV-vis absorption spectra in the multilayer buildup process. Red lines: spectra for the films after deposition of Au NPs; Blue lines: spectra for the films after deposition of titania nanosheets. The deposition time of Au NPs was (a) 2 and (b) 20 min. Inset in (b) shows the photographs of respective samples consisting of n layers each of Au NPs and titania nanosheets.

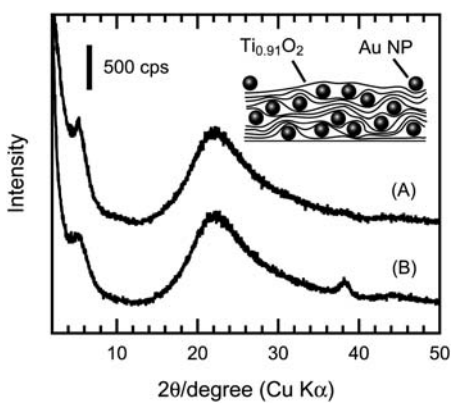

Fig. 5 XRD patterns for the multilayer assembly of glass/PEI/$Ti_{0.91}O_2$/PDDA/Au NP/(PDDA/$Ti_{0.91}O_2$/PDDA/Au NP)$_{11}$. The deposition time of Au NPs was (A) 2 and (B) 20 min. Inset shows a schematic illustration of Au NPs involved in the multilayer structure of corrugated titania nanosheets.

but coalesce into larger ones upon the adsorption onto the substrates covered with a PDDA layer, as described above.

On the other hand, the peak observed at $2\theta = 5.4°$ is assignable to the diffraction from the layered structure of titania nanosheets (Fig. 5), and the interlayer distance between titania nanosheets for the films of 2 min deposition was estimated to be 1.6 nm, which is similar to that for multilayer films composed of titania nanosheets and PDDA layers without Au NPs.[21b] These results suggest that the Au NPs are not pillars supporting the multilayer structure of titania nanosheets, but that the Au NPs are involved in the multilayer structure of corrugated nanosheets as shown in the inset of Fig. 5. A similar structure has been reported for the multilayer films composed of Al_{13} polyoxocations and MnO_2 nanosheets.[28] This model is reasonable since the diffraction peak is observed even for three layers of titania nanosheets without Au NPs. For the films of 20 min deposition, the diffraction peak was slightly broader and was observed at a lower angle ($2\theta = 5.2°$, corresponding to the interlayer distance of 1.7 nm). These results are suggestive of slightly disordered layers, likely due to larger NP size and smaller interparticle spacing, which cause poorer fitting between the layers.

Control of plasmon resonance by nanosheet coating

The thickness of a titania nanosheet layer covering Au NPs can be controlled by repeating the deposition of nanosheets. In order to estimate the decay length of electric field of Au NPs, we fabricated glass/PEI/$Ti_{0.91}O_2$/PDDA/Au NP/(PDDA/$Ti_{0.91}O_2$)$_n$ ($n = 1$–8, adsorption time of Au NPs: 20 min) and examined their LSPR properties (Fig. 6). The first layer of titania nanosheets on Au NPs enhanced the plasmon resonance as described above, and the enhancement factor, which we define as the ratio of absorbance after coverage with the single titania nanosheet layer to that before the coverage, were ~1.4 and ~2.0 at the peak wavelength and 800 nm, respectively. The enhancement factor decreased with increasing the number of nanosheet layers and became constant for the fourth and subsequent deposition (Fig. 6b). The initial enhancement is mainly ascribable to the increase of local refractive index as mentioned above. We ascribe the following small and constant enhancement to Rayleigh scattering since the absorbance increment is more significant in a shorter wavelength region, which gives rise to the apparent, slight blueshift of the peak wavelength after the fourth deposition (Fig. 6a). Since the mean thickness of a $Ti_{0.91}O_2$/PDDA layer was about 1.5 nm as estimated from the XRD peak appeared at $2\theta = 6.0°$, the electric field around the Au NPs decays within 3.0–4.5 nm of the nanosheet layers. The decay length for Au NPs with the size of 13.9 and 20.2 nm adsorbed on glass substrates was about 15 and 20 nm, respectively, in poly(methyl methacrylate).[10b] In the present system, it is also shown that the decay length of electric field is similar to the size of Au NPs. Therefore, the Au NPs covered with 1 or 2 layers of titania nanosheets would be useful for applications in which enhanced LSPR is advantageous, as described below.

Control of plasmon coupling

We also stacked Au NP layers with controlled interlayer distance so as to study effects of the interparticle distance on the interlayer plasmon coupling (Fig. 7). Although the plasmon absorption peak appeared at ~590 nm for the first layer of Au NPs, six layers of Au NPs with intervening PDDA layers without titania

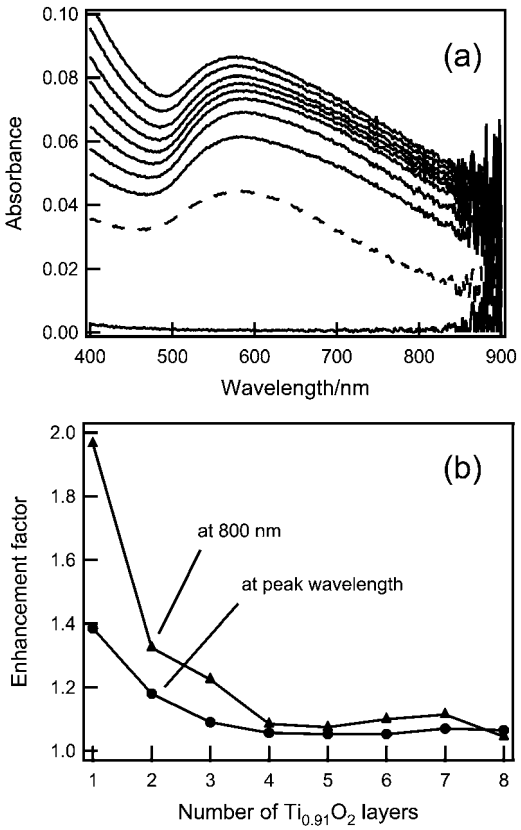

Fig. 6 (a) UV-vis absorption spectra in the buildup process of the multilayer films, glass/PEI/$Ti_{0.91}O_2$/PDDA/Au NP/(PDDA/$Ti_{0.91}O_2$)$_n$. Broken line: spectrum for the film after deposition of Au NPs; solid lines: spectra for the films after deposition of titania nanosheets. The deposition time of Au NPs was 20 min. (b) Enhancement factors of absorption at peak wavelength and at 800 nm by the coverage of Au NPs with titania nanosheets plotted against the number of titania nanosheet layers.

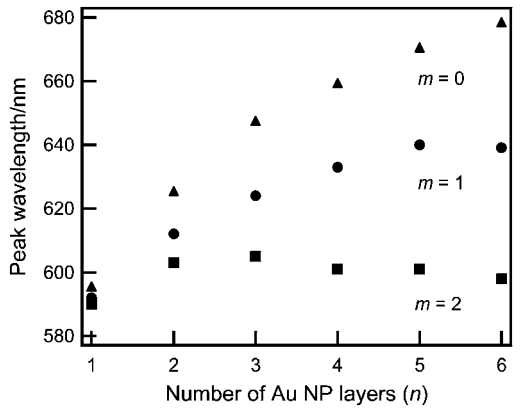

Fig. 7 Wavelength of the plasmon absorption peak plotted against the number (n) of layers of Au NPs in the films of glass/PEI/$Ti_{0.91}O_2$/PDDA/Au NP/((PDDA/$Ti_{0.91}O_2$)$_m$/PDDA/Au NP)$_{n-1}$. The number (m) of titania nanosheets was 0, 1, and 2. The deposition time of Au NPs was 20 min.

nanosheets (glass/PEI/$Ti_{0.91}O_2$/(PDDA/Au NP)$_6$) showed the peak at ~680 nm. The strong redshift is explained in terms of the interlayer plasmon coupling. When the six layers of Au NPs were stacked with intervening single titania nanosheet layers (glass/PEI/$Ti_{0.91}O_2$/PDDA/Au NP/(PDDA/$Ti_{0.91}O_2$/PDDA/Au NP)$_5$), the plasmon absorption peaked at ~640 nm. In the case of doubled nanosheet layers (glass/PEI/$Ti_{0.91}O_2$/PDDA/Au NP/((PDDA/$Ti_{0.91}O_2$)$_2$/PDDA/Au NP)$_5$), the peak shifted only slightly, from ~590 to ~600 nm, indicating that the plasmon coupling was almost suppressed by two titania nanosheets and three PDDA layers (total thickness: ~3.5 nm). This result is consistent with the decay length of electric field estimated above. Thus, to enhance and redshift the resonance peak, intervention of a single nanosheet layer is favorable. On the other hand, to integrate Au NPs without undue redshifts, two or three nanosheet layers must intervene in the Au NP layers.

Photovoltaic properties of assembled films

We examined the photovoltaic properties of the assembled films prepared on ITO substrates. A photocurrent was not generated from glass/ITO/PEI/($Ti_{0.91}O_2$/PDDA)$_n$/Au NP (n = 1, 5 and 10) electrodes under visible light (460 nm < λ < 700 nm) in an electrolyte containing TEOA as an electron donor, probably because the electron transfer from Au NPs to ITO *via* titania nanosheets was blocked by the insulating PEI and PDDA layers. When the electrodes were annealed at 500 °C for 1 h to remove the polymer layers,[29] it was observed by AFM that the size of Au NPs and their interparticle distance increased and the shape of the Au NPs became smoother and more spherical (Fig. 9a, inset). Decreases in fwhm of XRD peaks support the growth of Au NPs upon annealing. The broad absorption peak before annealing became sharper and blueshifted from 650 to 592 nm upon annealing, probably due to loss of particle anisotropy and loss of plasmon coupling, the latter of which was caused by an increase of interparticle distance. The XRD peaks of the n = 5 and 10 films at 5.2–5.4° disappeared, suggesting loss of the layered structures accompanying transition to the anatase phase as reported previously.[30] It is also known that a single layer of titania nanosheets retains its structure even at 500 °C.[30] All the annealed electrodes generated anodic photocurrents under visible light (460 nm < λ < 700 nm) (Fig. 8a). We have reported elsewhere that the photoinduced electron transfer occurs from Au NPs to anatase TiO_2.[7] Here we found that electron transfer to a single layer of titania nanosheets is also possible. As the thickness of

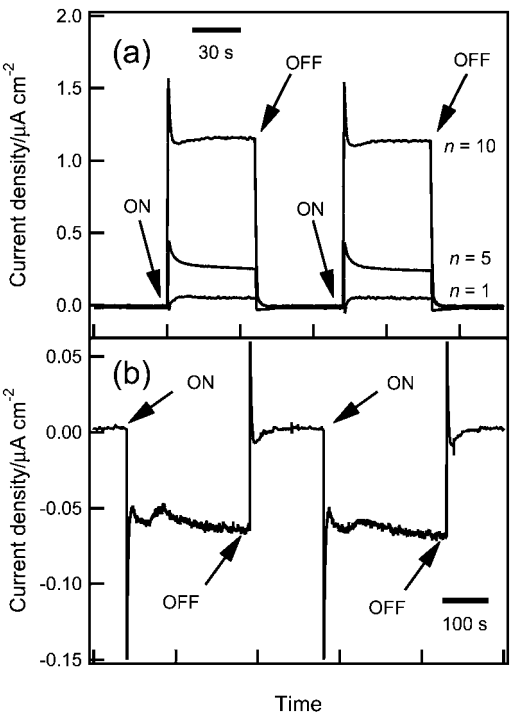

Fig. 8 Photocurrent responses of (a) glass/ITO/PEI/($Ti_{0.91}O_2$/PDDA)$_n$/Au NP and (b) glass/ITO/PEI/PSS/PDDA/Au NP/(PDDA/$Ti_{0.91}O_2$)$_{10}$ electrodes after annealing at 500 °C for 1 h in acetonitrile containing 0.74 M TEOA and 0.01 M TBAP under 460–700 nm light (200 mW cm^{-2}). The deposition time of Au NPs was 24 h.

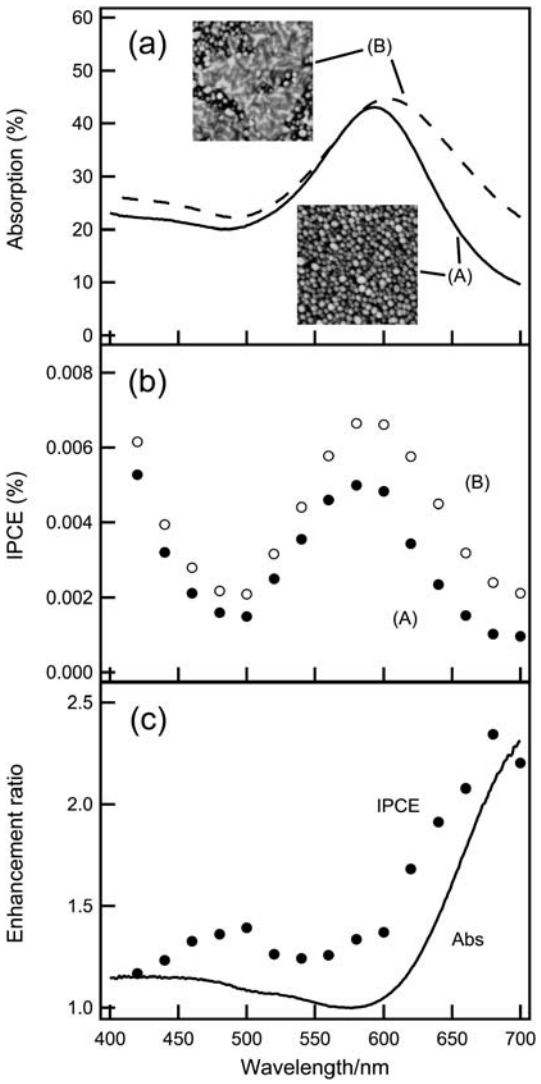

Fig. 9 (a) UV-vis absorption spectra and (b) photocurrent action spectra for the films, (A) glass/ITO/PEI/($Ti_{0.91}O_2$/PDDA)$_{10}$/Au NP and (B) glass/ITO/PEI/($Ti_{0.91}O_2$/PDDA)$_{10}$/Au NP/PDDA/$Ti_{0.91}O_2$, annealed at 500 °C for 1 h. The deposition time of Au NPs was 24 h. (c) Enhancement factor of IPCE and absorption plotted against wavelength. Inset in (a) shows AFM images (1 μm × 1 μm) of the corresponding samples.

titania increased, the anodic photocurrent also increased, probably because the electric field within the TiO_2 space charge layer facilitated transport of photoinjected electrons toward the bulk of titania and the recombination was suppressed. The conduction band edge of anatase is more positive than that of titania nanosheets by 0.1 V.[31] This may also contribute to the larger photocurrent for the glass/ITO/TiO_2(anatase)/Au NP electrodes.

As described above, coverage of Au NPs with titania nanosheets enhances plasmon absorption. We therefore examined effects of the enhancement on the photocurrents. The glass/ITO/PEI/$(Ti_{0.91}O_2$/PDDA$)_{10}$/Au NP electrode and that coated with a single layer of titania nanosheets were annealed at 500 °C for 1 h, and the absorption peaks of the electrodes became sharp and blueshifted by 60–70 nm. As expected from the previous results,[30] the sheet-like morphology of titania nanosheets covering Au NPs were maintained even after annealing as observed in AFM images (Fig. 9a, inset). Fig. 9 shows the absorption spectra and photocurrent (indicated as incident photon-to-electron conversion efficiency, IPCE) action spectra for the annealed electrodes. Both of the absorption and photocurrents were enhanced by the nanosheet overlayer especially in the longer wavelength region. Fig. 9c shows that the spectrum of the enhancement factor for absorption is in good agreement with that for photocurrents, indicating that the enhancement of photocurrents is mainly ascribable to the enhancement of plasmon absorption due to the increased refractive index around the Au NPs. Slightly higher enhancement factor for photocurrents could be due to a possible effect that the nanosheet overlayer suppresses recombination of excited electrons with electron acceptors in the electrolyte.

When the Au NPs on an ITO electrode were covered with ten layers of titania nanosheets (glass/ITO/PEI/PSS/PDDA/Au NP/(PDDA/$Ti_{0.91}O_2)_{10}$) and annealed at 500 °C, the electrode showed the reverse polarity of photoresponses, *i.e.*, cathodic photocurrents (Fig. 8b) and positive photopotentials in an electrolyte containing oxidized TEOA. This is because the photoresponses are based on the photoinduced electron transfer from plasmon excited Au NPs to TiO_2.[7f] In the case of the glass/ITO/TiO_2(anatase)/Au NP/$Ti_{0.91}O_2$ electrode shown above, incidentally, the nanosheet overlayer is too thin to take a sufficient amount of electrons from Au NPs, whereas the TiO_2 underlayer is thick enough to take electrons. Thus we could easily control the polarity of photoresponses by changing the layering order of Au NPs and titania nanosheets.

Conclusions

We have successfully fabricated the layer-by-layer assembled multilayer films composed of Au NPs and titania nanosheets in an arbitrary order. We have examined the plasmon resonance properties of Au NPs covered with a multilayer of titania nanosheets and clarified that the coverage enhances the plasmon resonance and that the electric field of Au NPs decays within 2 to 3 layers of nanosheets. Plasmon coupling between Au NPs is therefore almost suppressed with 2 layers of intervening titania nanosheets. The coverage of Au NPs with a single layer of titania nanosheets is found to enhance the plasmon resonance-based photoelectric conversion properties. The polarity of photoresponses can be controlled by changing the order of layer-by-layer assembly of Au NPs and titania nanosheets.

Acknowledgements

This work was financially supported in part by KAKENHI (Grant-in-Aid for Scientific Research) on Priority Area "Strong Photon-Molecule Coupling Fields (No. 470)" from MEXT of Japan (No. 19049008 for TT), KAKENHI (No. 17350064 for TT and No. 18759001 for NS) from JSPS and MEXT, respectively, and CREST of JST.

Notes and references

1 (*a*) P. Mulvaney, *Langmuir*, 1996, **12**, 788; (*b*) J. Pérez-Juste, I. Pastoriza-Santos, L. M. Liz-Marzán and P. Mulvaney, *Coord. Chem. Rev.*, 2005, **249**, 1870; (*c*) K. L. Kelly, E. Coronado, L. L. Zhao and G. C. Schatz, *J. Phys. Chem. B*, 2003, **107**, 668.

2 (*a*) A. J. Haes, S. Zou, G. C. Schatz and R. P. Van Duyne, *J. Phys. Chem. B*, 2004, **108**, 109; (*b*) M. M. Miller and A. A. Lazarides, *J. Phys. Chem. B*, 2005, **109**, 21556; (*c*) Z.-m. Qi, I. Honma and H. Zhou, *Opt. Lett.*, 2006, **31**, 1854; (*d*) N. Nath and A. Chilkoti, *Anal. Chem.*, 2002, **74**, 504; (*e*) R. Bukasov and J. S. Shumaker-Parry, *Nano Lett.*, 2007, **7**, 1113.

3 (*a*) S. Nie and S. R. Emory, *Science*, 1997, **275**, 1102; (*b*) R. F. Aroca, P. J. G. Goulet, D. S. dos Santos Jr., R. A. Alvarez-Puebla and O. N. Oliveira Jr., *Anal. Chem.*, 2005, **77**, 378; (*c*) S. Yun, Y.-K. Park, S. K. Kim and S. Park, *Anal. Chem.*, 2007, **79**, 8584.

4 (*a*) W. Knoll, M. R. Philpott and W. G. Golden, *J. Chem. Phys.*, 1982, **77**, 219; (*b*) M. Osawa, *Bull. Chem. Soc. Jpn.*, 1997, **70**, 2861.

5 (*a*) I. H. El-Sayed, X. Huang and M. A. El-Sayed, *Nano Lett.*, 2005, **5**, 829; (*b*) X. Huang, I. H. El-Sayed, W. Qian and M. A. El-Sayed, *J. Am. Chem. Soc.*, 2006, **128**, 2115; (*c*) F. Nakamura, M. Ito, A. Manna, K. Tamada, M. Hara and W. Knoll, *Jpn. J. Appl. Phys.*, 2006, **45**, 1026.

6 (*a*) Y. Ohko, T. Tatsuma, T. Fujii, K. Naoi, C. Niwa, Y. Kubota and A. Fujishima, *Nat. Mater.*, 2003, **2**, 29; (*b*) K. Naoi, Y. Ohko and T. Tatsuma, *J. Am. Chem. Soc.*, 2004, **126**, 3664; (*c*) K. Kawahara, K. Suzuki, Y. Ohko and T. Tatsuma, *Phys. Chem. Chem. Phys.*, 2005, **7**, 3851; (*d*) K. Matsubara and T. Tatsuma, *Adv. Mater.*, 2007, **19**, 2802; (*e*) K. Matsubara, K. L. Kelly, N. Sakai and T. Tatsuma, *J. Mater. Chem.*, 2009, **19**, 5526.

7 (*a*) Y. Tian and T. Tatsuma, *Chem. Commun.*, 2004, 1810; (*b*) Y. Tian and T. Tatsuma, *J. Am. Chem. Soc.*, 2005, **127**, 7632; (*c*) K. Yu, Y. Tian and T. Tatsuma, *Phys. Chem. Chem. Phys.*, 2006, **8**, 5417; (*d*) K. Yu, N. Sakai and T. Tatsuma, *Electrochemistry*, 2008, **76**, 161; (*e*) Y. Takahashi and T. Tatsuma, *Electrochem. Commun.*, 2008, **10**, 1404; (*f*) N. Sakai, Y. Fujiwara, Y. Takahashi and T. Tatsuma, *ChemPhysChem*, 2009, **10**, 766.

8 E. Kowalska, R. Abe and B. Ohtani, *Chem. Commun.*, 2009, 241.

9 T. Tatsuma, K. Takada and T. Miyazaki, *Adv. Mater.*, 2007, **19**, 1249.

10 (*a*) M. Brust, D. Bethell, C. J. Kiely and D. J. Schiffrin, *Langmuir*, 1998, **14**, 5425; (*b*) T. Okamoto, I. Yamaguchi and T. Kobayashi, *Opt. Lett.*, 2000, **25**, 372; (*c*) J.-E. Park, T. Momma and T. Osaka, *Electrochim. Acta*, 2007, **52**, 5914.

11 (*a*) S. Toyama, O. Takei, M. Tsuge, R. Usami, K. Horikoshi and S. Kato, *Electrochem. Commun.*, 2002, **4**, 540; (*b*) D. van Noort and C.-F. Mandenius, *Biosens. Bioelectron.*, 2000, **15**, 203; (*c*) Y. Tian, H. Liu, G. Zhao and T. Tatsuma, *J. Phys. Chem. B*, 2006, **110**, 23478; (*d*) N. Sakai, Y. Fujiwara, M. Arai, K. Yu and T. Tatsuma, *J. Electroanal. Chem.*, 2009, **628**, 7.

12 (*a*) A. Gole, C. J. Orendorff and C. J. Murphy, *Langmuir*, 2004, **20**, 7117; (*b*) Y. Niidome, H. Takahashi, S. Urakawa, K. Nishioka and S. Yamada, *Chem. Lett.*, 2004, **33**, 454; (*c*) C. Lu, H. Möhwald and A. Fery, *J. Phys. Chem. C*, 2007, **111**, 10082; (*d*) T. Ung, L. M. Liz-Marzán and P. Mulvaney, *J. Phys. Chem. B*, 2001, **105**, 3441; (*e*) S. Vial, I. Pastoriza-Santos, J. Pérez-Juste and L. M. Liz-Marzán, *Langmuir*, 2007, **23**, 4606; (*f*) A. Gole and C. J. Murphy, *Chem. Mater.*, 2005, **17**, 1325; (*g*) Y. H. Su, W. H. Lai, L. G. Teoh, M. H. Hon and J. L. Huang, *Appl. Phys. A: Mater. Sci. Process.*, 2007, **88**, 173.

13 G. Decher, *Science*, 1997, **277**, 1232.

14 (*a*) S. K. Ghosh and T. Pal, *Chem. Rev.*, 2007, **107**, 4797; (*b*) Z. Zhong, S. Patskovskyy, P. Bouvrette, J. H. T. Luong and A. Gedanken, *J. Phys. Chem. B*, 2004, **108**, 4046.

15 (*a*) M. Mitsuishi, M. Ishifuji, H. Endo, H. Tanaka and T. Miyashita, *Polym. J.*, 2007, **39**, 411; (*b*) M. Ishifuji, M. Mitsuishi and T. Miyashita, *Chem. Commun.*, 2008, 1058.
16 (*a*) T. Sasaki, *J. Ceram. Soc. Jpn.*, 2007, **115**, 9; (*b*) M. Osada and T. Sasaki, *J. Mater. Chem.*, 2009, **19**, 2503.
17 (*a*) T. Sasaki, M. Watanabe, H. Hashizume, H. Yamada and H. Nakazawa, *J. Am. Chem. Soc.*, 1996, **118**, 8329; (*b*) T. Sasaki and M. Watanabe, *J. Am. Chem. Soc.*, 1998, **120**, 4682; (*c*) T. Sasaki, Y. Ebina, Y. Kitami, M. Watanabe and T. Oikawa, *J. Phys. Chem. B*, 2001, **105**, 6116.
18 (*a*) Y. Zhou, R. Ma, Y. Ebina and T. Sasaki, *Chem. Mater.*, 2006, **18**, 1235; (*b*) Y. Zhou, L. Z. Wang, R. Ma, Y. Ebina, K. Takada and T. Sasaki, *Curr. Nanosci.*, 2007, **3**, 155.
19 (*a*) N. R. Jana, L. Gearheart and C. J. Murphy, *J. Phys. Chem. B*, 2001, **105**, 4065; (*b*) N. R. Jana, L. Gearheart and C. J. Murphy, *Langmuir*, 2001, **17**, 6782; (*c*) A. Gole and C. J. Murphy, *Chem. Mater.*, 2004, **16**, 3633.
20 (*a*) M. Hervieu and B. Raveau, *Rev. Chim. Miner.*, 1981, **18**, 642; (*b*) I. E. Grey, C. Li, I. C. Madsen and J. A. Watts, *J. Solid State Chem.*, 1987, **66**, 7; (*c*) M. Gateshki, S.-J. Hwang, D. H. Park, Y. Ren and V. Petkov, *Chem. Mater.*, 2004, **16**, 5153; (*d*) K. Fukuda, I. Nakai, C. Oishi, M. Nomura, M. Harada, Y. Ebina and T. Sasaki, *J. Phys. Chem. B*, 2004, **108**, 13088.
21 (*a*) T. Sasaki, Y. Ebina, M. Watanabe and G. Decher, *Chem. Commun.*, 2000, 2163; (*b*) T. Sasaki, Y. Ebina, T. Tanaka, M. Harada, M. Watanabe and G. Decher, *Chem. Mater.*, 2001, **13**, 4661.
22 K. C. Grabar, R. G. Freeman, M. B. Hommer and M. J. Natan, *Anal. Chem.*, 1995, **67**, 735.
23 S. Basu, S. K. Ghosh, S. Kundu, S. Panigrahi, S. Praharaj, S. Pande, S. Jana and T. Pal, *J. Colloid Interface Sci.*, 2007, **313**, 724.
24 M. Kanehara, J. Sakurai, H. Sugimura and T. Teranishi, *J. Am. Chem. Soc.*, 2009, **131**, 1630.
25 (*a*) P. N. Njoki, I.-I. S. Lim, D. Mott, H.-Y. Park, B. Khan, S. Mishra, R. Sujakumar, J. Luo and C.-J. Zhong, *J. Phys. Chem. C*, 2007, **111**, 14664; (*b*) J. D. Driskell, R. J. Lipert and M. D. Porter, *J. Phys. Chem. B*, 2006, **110**, 17444.
26 (*a*) K.-H. Su, Q.-H. Wei, X. Zhang, J. J. Mock, D. R. Smith and S. Schultz, *Nano Lett.*, 2003, **3**, 1087; (*b*) P. K. Jain, W. Huang and M. A. El-Sayed, *Nano Lett.*, 2007, **7**, 2080; (*c*) C. Tabor, R. Murali, M. Mahmoud and M. A. El-Sayed, *J. Phys. Chem. A*, 2009, **113**, 1946.
27 The small crystallite size is assumed to be the only case of line broadening. The Scherrer's equation: $D = K\lambda/\beta\cos\theta$, where D is the mean crystallite dimension, K the crystallite shape constant (0.9), θ the Bragg angle, λ the X-ray wavelength, and β the fwhm of the peak in radians.
28 L. Z. Wang, N. Sakai, Y. Ebina, K. Takada and T. Sasaki, *Chem. Mater.*, 2005, **17**, 1352.
29 T. Sasaki, Y. Ebina, K. Fukuda, T. Tanaka, M. Harada and M. Watanabe, *Chem. Mater.*, 2002, **14**, 3524.
30 K. Fukuda, Y. Ebina, T. Shibata, T. Aizawa, I. Nakai and T. Sasaki, *J. Am. Chem. Soc.*, 2007, **129**, 202.
31 N. Sakai, Y. Ebina, K. Takada and T. Sasaki, *J. Am. Chem. Soc.*, 2004, **126**, 5851.

